Orientation dependence of core edges from anisotropic materials determined by inelastic scattering of fast electrons

R. D. Leapman,* P. L. Fejes,† and J. Silcox
School of Applied and Engineering Physics and The Materials Science Center, Clark Hall, Cornell University, Ithaca, New York 14853
(Received 8 April 1983)

Electron-energy-loss spectra have been measured in the region of the K edges in graphite and hexagonal boron nitride. The fine structure is found to be strongly dependent on the crystal orientation and momentum transfer. Angular distributions of peaks in the spectrum have been recorded from crystals with the c axis parallel and at 45° to the beam direction. These agree well with the theoretical distributions for transitions to π^* and σ^* final states in a hybridized atomic-orbital model. Peaks in the energy-loss spectrum are compared with band calculations of the ground-state density of states. Some correspondence is found between these but there is also evidence of core excitons.

I. INTRODUCTION

Electron-energy-loss spectroscopy is an established technique for investigating electronic structure in solids. Excitation of core levels by fast electrons can be especially useful since the initial state involved in the transition is relatively simple. Fine structure in the region of the core edges in energy-loss spectra can thus be attributed predominantly to features associated with unoccupied conduction states.[1–6] Peaks in the spectrum arising from valence-electron excitation, on the other hand, involve the more complicated joint density of states between occupied and unoccupied portions of the bands as well as collective plasmon resonances.[7–12] In the present work we report the observation of an orientation dependence of core edges in anisotropic materials. We show how energy-loss measurements near the K edges in graphite and hexagonal boron nitride give information about electronic structure by recording spectra as a function of scattering angle and crystal orientation. Some earlier reported orientation-dependence studies of core edges using absorption of polarized synchrotron radiation are discussed in the context of our results for boron nitride.[13] Other orientation-dependence studies of photoabsorption spectra in anisotropic crystals have been also reported for layered dichalcogenides.[14,15] Energy-loss measurements have been reported previously for core edges in graphite and boron nitride.[3,4,16–18] In the case of graphite a few measurements have also been recorded at different scattering angles.[18] However, our experiments are the first demonstration in detail that the orientation dependence for fast electrons can be exploited to give information about electronic structure.

II. DIPOLE MATRIX ELEMENTS

Fine structure in the electron-energy-loss spectrum can arise when an inner-shell electron in a state $|i\rangle$ makes a transition to an unoccupied state $|f\rangle$ characterized by a high combined value of density of states and matrix element factors. The cross section, differential in energy loss E and solid angle Ω, for the excitation process can be written within the first Born approximation and the independent electron model as[19]

$$\frac{d^2\sigma_{if}(\theta)}{d\Omega\, dE}=\frac{4}{a_0^2 q^4}\,|\langle f|\exp(i\vec{q}\cdot\vec{r})|i\rangle|^2\,, \tag{1}$$

where $\vec{q}$ is the momentum transfer and a_0 is the Bohr radius. The final state is normalized per unit energy range. For incident electron energy E_0 and corresponding wave vector $\vec{k}$, the momentum transfer $\vec{q}$ is related to the scattering angle θ through conservation of energy and momentum (see Fig. 1) by

$$q^2=k^2(\theta^2+\theta_E^2)\,, \tag{2}$$

where $\theta_E=E/2E_0$ and $E_0=\hbar^2k^2/2m$. The operator in Eq. (1) can be expanded as

$$\exp(i\vec{q}\cdot\vec{r})=1+\vec{q}\cdot\vec{r}-i(\vec{q}\cdot\vec{r})^2+\cdots\,,$$

so provided that $|\vec{q}\cdot\vec{r}|\ll 1$, and that $|i\rangle$ and $|f\rangle$ are

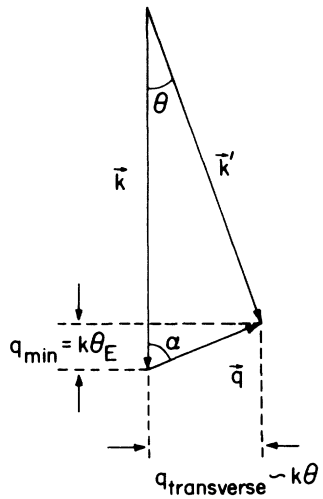

FIG. 1. Scattering diagram showing the incident electron momentum $\vec{k}$ and the momentum transfer $\vec{q}$ for scattering angle θ. The minimum (parallel) and transverse momentum transfers are also indicated.

orthogonal (i.e., we are in a single-particle picture), the matrix element reduces to the dipole form. If r_c is the radius of the core we require that $q \ll (1/r_c)$. This condition can be shown to be equivalent to $q \ll (2m_0E_c)^{1/2}/\hbar$, where E_c is the core binding energy.[20] In terms of the scattering angles of the order of θ we have $\theta \ll (E_c/E_0)^{1/2}$. In the present work we are interested in scattering angles of the order of $\theta_E \sim (E_c/2E_0)$. For 75-keV electrons and core shells with binding energies $\sim$200–300 eV, we have $\theta_E \sim 2\times10^{-3}$ rad and $(E_c/E_0)^{1/2} \sim 6\times10^{-2}$ rad. The condition for the validity of the dipole approximation is therefore easily satisfied. We can now replace the matrix element in Eq. (1) by $iq\langle f \mid \hat{\epsilon}_q\cdot\vec{r} \mid i\rangle$, where $\hat{\epsilon}_q$ is a unit vector in the direction of $\vec{q}$. In this form the matrix element is similar to the dipole matrix element for the absorption of polarized electromagnetic radiation which, again assuming the one-electron model, is given by[21]

$$\sigma_{\text{absorption}}(\nu) \propto |\langle f \mid \exp(i\vec{q}_\nu\cdot\vec{r})\hat{e}\cdot\vec{r} \mid i\rangle|^2 , \tag{3}$$

where $\vec{q}_\nu$ is now the momentum of an incident photon of energy $h\nu$, $\hat{e}$ is the polarization unit vector of the electric field, and $\vec{r}$ is the coordinate of the atomic electron involved in the transition. Thus even in the case of photoabsorption some assumption is necessary about the size of the momentum transfer. This involves approximation of the exponential in Eq. (3) by unity, otherwise the matrix element cannot be written in the pure dipole form. For the inner-shell excitations considered in this work, the momentum transfer in the photoabsorption processes is actually of the same order as in the electron-energy-loss process ($\sim$0.1 Å^{-1}).

In a solid, or in particular an anisotropic crystal, the final state $|f\rangle$ has definite directionality. This means that in an electron-energy-loss experiment the matrix element depends on the orientation of $\hat{\epsilon}_q$ with respect to the crystal axes. The direction of $\hat{\epsilon}_q$ is determined by the scattering angle as shown in Fig. 2, while the direction of the crystal axes can be selected independently by rotating the sample through angle γ (Fig. 2). Variations of the matrix element may therefore be studied by recording spectra both as a function of scattering angle and crystal orientation. It is noted that the energy-loss technique probes states polarized parallel to the incident beam when the scattering angle is zero. Absorption of synchrotron radiation probes states polarized along the electric field direction, i.e., perpendicular to the incident x rays.

To consider the behavior of the matrix elements in more detail we need a model for the unoccupied final states in the crystal. Let us adopt for the present a tight-binding model where the wave functions $|f\rangle$ can be expressed as Bloch functions[22] with the atomic orbitals chosen as a basis set in the expansion. Because of the small spatial extent of the initial state, the dominant contribution to the matrix element is due to the overlap between the initial state and that part of the tight-binding $|f\rangle$ representing the atomic state localized on the same atom. Thus we shall neglect contributions to the matrix element from atomic states in $|f\rangle$ localized on the other atoms. This model is essentially atomic but we note that band-structure effects will be reflected in the energies of the final states and the corresponding density of states. These will determine the energy dependence of the spectrum above the core edges. The dipole form of the matrix element requires that under the above approximations optical selection rules will apply, i.e., the relation between angular momentum in the initial state (l) and final state (l') is $l' = |l\pm1|$. It is the angular part of the final state that is dependent on l, so for an initial s symmetry the final symmetry must be p. In a solid the orientation of the angular parts of the wave functions will reflect local fields and thus the crystal structure. If it is assumed that the radial and angular parts of the final state are separable, calculation of the angular part of the matrix element can be performed and this will determine the orientation and scattering angle dependence of the spectrum.

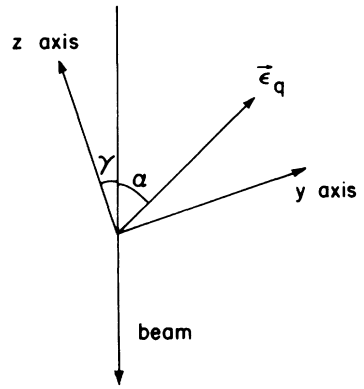

FIG. 2. Scattering geometry showing the angle that the incident beam makes with the crystal z axis and the direction of momentum transfer (γ and α, respectively).

Let us therefore write

$$|i\rangle = R_{n_il_i}(r)Y_{l_im_i}(\beta,\phi) ,$$

$$|f\rangle = R_{n_fl_f}(r)Y_{l_fm_f}(\beta,\phi) ,$$

$$\vec{r} = r\hat{\epsilon}_r(\beta,\phi) .$$

Here $\vec{r}$ is the spherical coordinate (r,β,ϕ), $\hat{\epsilon}_r$ is a unit vector along $\vec{r}$, i.e., the angular coordinate (β,ϕ), $R_{nl}(r)$ is a radial wave function, and Y_{lm} is a spherical harmonic. Then

$$\langle f \mid \hat{\epsilon}_q\cdot\vec{r} \mid i\rangle = \int_r R_{n_fl_f}(r)r^3R_{n_il_i}(r)dr \int_{\phi\beta} (\hat{\epsilon}_q\cdot\hat{\epsilon}_r)Y_{l_im_i}(\beta,\phi)Y_{l_fm_f}(\beta,\phi)\sin\beta\, d\beta\, d\phi . \tag{4}$$

It is seen that the scalar product $\hat{\epsilon}_q\cdot\hat{\epsilon}_r$ in Eq. (4) depends on the tilt angle between the incident beam and the crystal axes γ and the angle α between the incident beam and the momentum-transfer direction (Fig. 2).

III. GRAPHITE AND BORON NITRIDE

Both graphite and hexagonal boron nitride are highly anisotropic crystals having hexagonal layered structures.

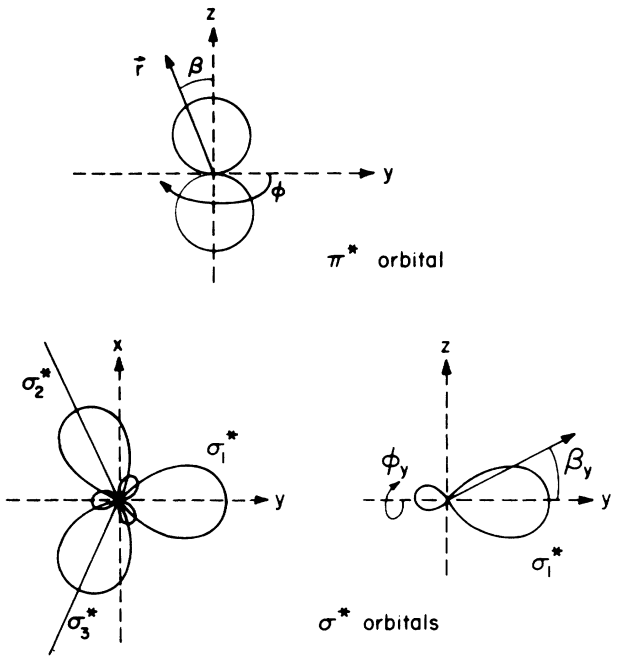

FIG. 3. Spherical and Cartesian coordinates for the π^* and σ^* orbitals in graphite and hexagonal boron nitride.

In terms of atomic orbitals, these materials have three hybridized $2sp_xp_y(\sigma)$ orbitals per atom in the layer plane and one $p_z(\pi)$ orbital per atom perpendicular to the layers. These represent the bonding orbitals but there are also antibonding σ^* and π^* states which can be constructed from different combinations of the atomic orbitals.

The initial $1s$ state has no angular dependence and is only a function of r in the spherical coordinate system. The π^* state is taken to be p_z atomic orbital which has an angular part $\sim\cos\beta$ (see Fig. 3). Noting that

$$\hat{\epsilon}_q\cdot\hat{\epsilon}_r=\sin\beta\sin(\alpha-\gamma)\cos\phi+\cos\beta\cos(\alpha-\gamma)\ ,$$

and that the angular part of Eq. (4) then is $\langle 1s\,|\,\hat{\epsilon}_q\cdot\hat{\epsilon}_r\,|\,p_z\rangle\propto\cos(\alpha-\gamma)$, the cross section [Eq. (1)] becomes

$$\frac{d^2\sigma_\pi(\theta,\gamma)}{d\Omega\,dE}\propto\frac{\cos^2(\alpha-\gamma)}{q^2}\propto\frac{\cos^2[\tan^{-1}(\theta/\theta_E)-\gamma]}{\theta^2+\theta_E^2}\ . \tag{5}$$

In the special case $\gamma=0$, (i.e., normal incidence), the differential cross section for the $1s\rightarrow\pi^*$ transition reduces to

$$\frac{d^2\sigma_\pi(\theta,0)}{d\Omega\,dE}\propto\frac{\theta_E^2}{(\theta^2+\theta_E^2)^2}\ . \tag{6}$$

The σ^* orbitals in graphite or hexagonal boron nitride can be made up in this model by appropriate sums of $2s$, $2p_x$, and $2p_y$ atomic orbitals.

First assume that $|\sigma_1^*\rangle=3^{-1/2}(|2s\rangle+\sqrt{2}\,|2p_y\rangle)$ is in the plane containing z and $\hat{\epsilon}_q$. We define β_y and θ_y in order to carry out the angular integration for the $|\sigma_1^*\rangle$ orbital (Fig. 3). Thus

$$\hat{\epsilon}_q\cdot\hat{\epsilon}_r=-\sin(\alpha-\gamma)\cos\beta_y+\cos(\alpha-\gamma)\sin\beta_y\cos\phi_y\ .$$

The integration over the angular part of Eq. (4) gives

$$\langle 1s\,|\,\hat{\epsilon}_q\cdot\hat{\epsilon}_r\,|\,\sigma_1^*\rangle\propto\sin(\alpha-\gamma)\ .$$

Now we consider transitions to $|\sigma_2^*\rangle$ and $|\sigma_3^*\rangle$. Clearly the $|2s\rangle$ parts of these orbitals cannot contribute because of symmetry. Furthermore, symmetry requires that the contribution of the $|1s\rangle\rightarrow|2p_x\rangle$ transition be also zero since $|p_x\rangle$ is perpendicular to $\hat{\epsilon}_q$ (Fig. 3). Thus

$$\frac{d^2\sigma_\sigma(\theta,\gamma)}{d\Omega\,dE}\propto\frac{\sin^2(\alpha-\gamma)}{q^2}\propto\frac{\sin^2[\tan^{-1}(\theta/\theta_E)-\gamma]}{\theta^2+\theta_E^2}\ . \tag{7}$$

This same result can be shown to hold in the general case where $|\sigma_1^*\rangle$ is not in the plane containing z and $\hat{\epsilon}_q$. For normal incidence when $\gamma=0$, the differential cross section for the $1s\rightarrow\sigma^*$ transition reduces to

$$\frac{d^2\sigma_\sigma(\theta,0)}{d\Omega\,dE}\propto\frac{\theta^2}{(\theta^2+\theta_E^2)^2}\ . \tag{8}$$

IV. EXPERIMENTAL CONSIDERATIONS

The preceding section has shown us that to investigate the orientation dependence of core edges we must probe the scattering on an angular scale commensurate with θ_E. For the boron K edge (192 eV) and the carbon K edge (285 eV) with 75-keV incident electrons, θ_E has the values 1.3×10^{-3} and 2×10^{-3} rad, respectively. An angular

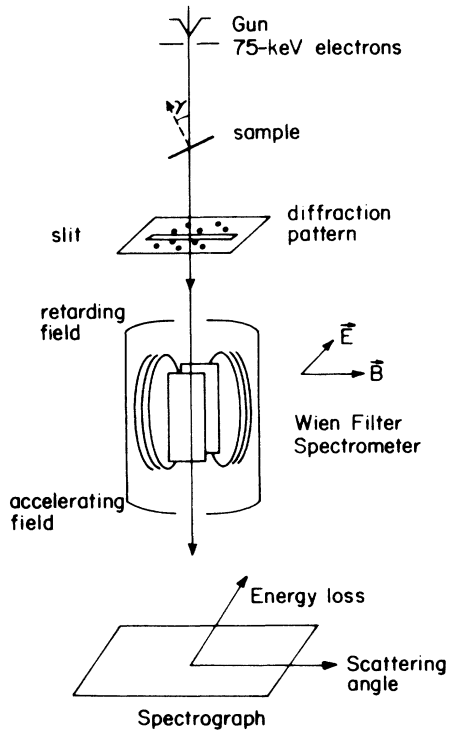

FIG. 4. Schematic diagram of apparatus showing the arrangement of the electron microscopic and the Wien filter spectrometer.

resolution of order 2×10^{-4} rad is therefore desirable to explore these effects. It is worth noting that at these angles, the momentum transfer is much less than the Brillouin-zone boundary so that changes as a result of band-structure variations should not arise over the angles of interest. This may not be true for deeper core losses.

Such conditions are readily achievable in an electron-microscope—electron-spectrometer system described previously.[23] With the use of the electron microscope in the selected area diffraction mode a 4-μm spot of 75-keV electrons is incident on the specimen with a beam divergence of $\sim2\times10^{-4}$ rad. The diffraction pattern is viewed on a fluorescent screen and can be recorded on photographic plates. An entrance slit to the Wien filter spectrometer selects electrons according to their scattering angle and the spectrometer disperses them in a direction perpendicular to the slit (see Fig. 4). A two-dimensional pattern results, giving a map of the scattered electron intensity as a function of both energy loss and scattering angle. The optical density of a photographic plate exposed appropriately to electrons is to a good approximation linear with the electron intensity and profiles can be obtained with a densitometer. Some digital scans of the energy-loss spectrum were also recorded. Pulses originating from a scintillator-photomultiplier were passed to a discriminator before being counted and recorded directly by a computer. In this case the angular resolution was not as high as for photographic recording because of the finite size of the scintillator aperture and the noise was greater since the spectra were recorded serially. However, these scans provided a useful check of linearity of the densitometer traces from the photographic plates. Digital control of the scans made it possible to record scans parallel to the energy axis or parallel to the angular axis and to introduce alignment checks.

Specimens were inserted either in a standard holder for normal-incidence measurements or in a specially designed holder at 45° to the incident-beam direction. The azimuthal angle for the tilted samples was set by examining the diffraction pattern and rotating the sample to give the correct orientation. Samples of graphite were prepared by cleaving with adhesive tape. After dissolving the tape in chloroform the flakes were mounted on 3-mm copper grids. Thin films about 100–200 Å thick were obtained in this way. Boron nitride samples were prepared by grinding bulk BN and suspending the powder in ethanol. The liquid was picked up on a support film of $\sim$100-Å amorphous carbon, and after drying, flakes about 3 μm in diameter lying flat on the substrate were selected for study. Calibration of the scattering angles was carried out with the use of the diffraction pattern and the energy loss with the use of a digital offset to the Wien filter spectrometer. Absolute measurement of the energy losses was accurate to $\sim\pm0.5$ eV and spectra were recorded at an energy resolution of ~1.4 eV.

V. RESULTS

A. Graphite

Figures 5(a) and 5(b) show spectrographs recorded on photographic plates in the region of the carbon K edge for a thin ($\sim$200 Å) sample of graphite oriented with the c axis parallel to the incident-beam direction ($\gamma=0$) and at a tilt of $\gamma=45°$, respectively. The angular and energy scales are indicated so that two clear peaks in energy can be seen in both spectrographs at 285.5 and 292.5 eV. For normal

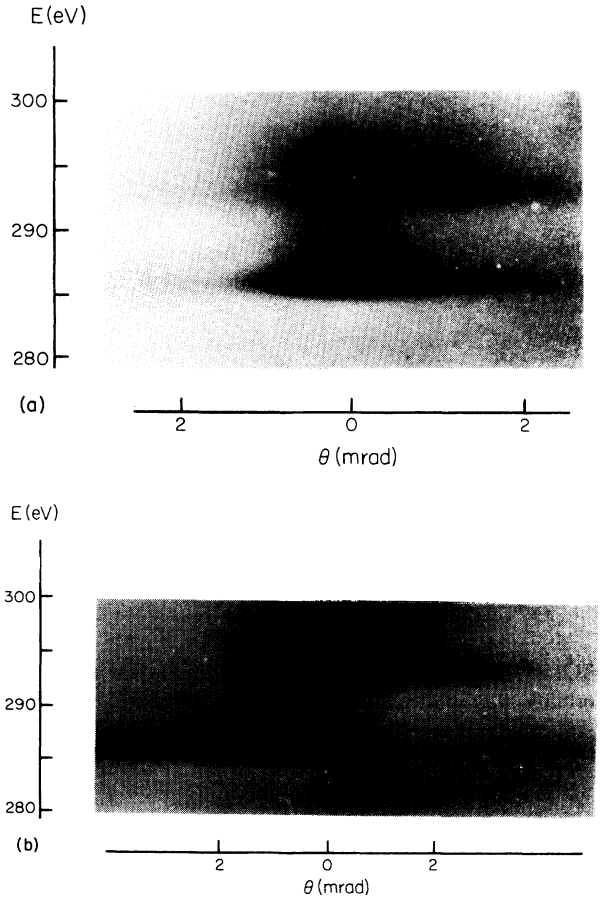

FIG. 5. (a) Spectrograph recorded on photographic plate at the carbon K edge in graphite oriented at normal incidence ($\gamma=0$). The angular and energy scales are indicated. (b) Spectrograph at the carbon K edge in graphite oriented with c axis at 45° to the incident beam direction ($\gamma=45°$).

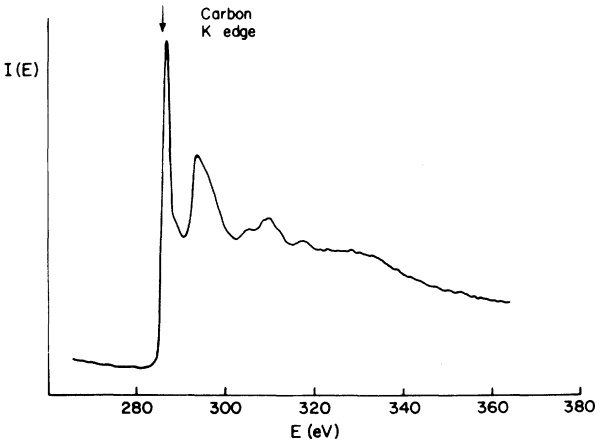

FIG. 6. Energy-loss spectrum recorded digitially at the carbon K edge in graphite oriented at normal incidence ($\gamma=0$).

incidence, the 285.5 eV peak is concentrated at smaller angles than the one at 292.5 eV, which shows a minimum at $\theta=0$. It is also seen that a weak tail from the 285.5-eV peak overlaps with the intensity in the peak at 292.5 eV. In the case of the 45° tilted sample the peaks are asymmetrical about $\theta=0$. Fine structure in the 1s core excitation spectrum of graphite has been reported previously for electrons incident parallel to the c axis.[4,17] The very sharp peak at the edge (285.5 eV) has been attributed to excitation to π^* states whereas the broader peak about 7 eV above threshold (292.5 eV) has been attributed to a $1s\rightarrow\sigma^*$ transition. This identification has been carried out by comparison of spectra with density of states derived from band calculations,[24] which we shall discuss later. We note that assignments of the 285.5- and 292.5-eV peaks as transitions to π^* and σ^* states are consistent with existing momentum dependence studies at normal incidence by Kincaid *et al.*[18]

Figure 6 shows a digital scan over a larger energy range of the carbon K edge in a thin graphite sample again about 100—200 Å thick oriented with c axis parallel to the incident beam. The same peaks seen in the spectrographs of Figs. 5(a) and 5(b) are observed and the spectrum is similar to that obtained by Kincaid *et al.*[18] at an incident energy of 200 keV. Peaks lying 50 eV or more above threshold may be attributed to backscattering of the ejected electron by neighboring atoms, i.e., extended x-ray absorption fine structure (EXAFS).[18,25–28] It is also noted that multiple inelastic scattering involving one or more plasmon excitations following inner-shell ionization can cause additional peaks in the spectrum for thicker samples. In general it may be necessary to carry out a deconvolution to remove such effects.[29,30] In the present work we are mainly concerned with structure within 10 or 20 eV of threshold and samples thin enough for these effects to be relatively small. The spectrum in Fig. 6 was recorded using a detector aperture such that the signal was integrated over a range of scattering angles, centered around $\theta=0$. The angular resolution was not as good as for the spectrograph recorded on photographic plates.

Let us now analyze our data in more detail. Figures 7(a) and 7(b) are microdensitometer traces across the energy axes of the spectrographs at different scattering angles for $\gamma=0$ and 45°, respectively. The spectra for normal incidence [Fig. 7(a)] show that as the scattering angle increases the π^* peak decreases relative to the σ^* peak. For the spectra at $\gamma=45°$ the microdensitometer traces in Fig. 7(b) show that at positive θ the π^* peak is strong and the σ^* weak while at negative θ this situation is reversed. In the normal-incidence spectra a weak maximum is visible at 306 eV as the scattering angle increases but is not evident at $\theta=0$. Another peak occurs at 310 eV which is strong at $\theta=0$ but falls off with increasing θ. Figure 8 shows microdensitometer traces along the scattering angle axis for the π^* and σ^* peaks in samples oriented at normal incidence. Traces were recorded at energy losses corresponding to the peak values (285.5 and 292.5 eV) and at energies just below the peaks (283 and 290 eV). In this way the background intensity could be subtracted from the signal. The weak bumps in the tails of both the signal and background traces were due to slight irregularities

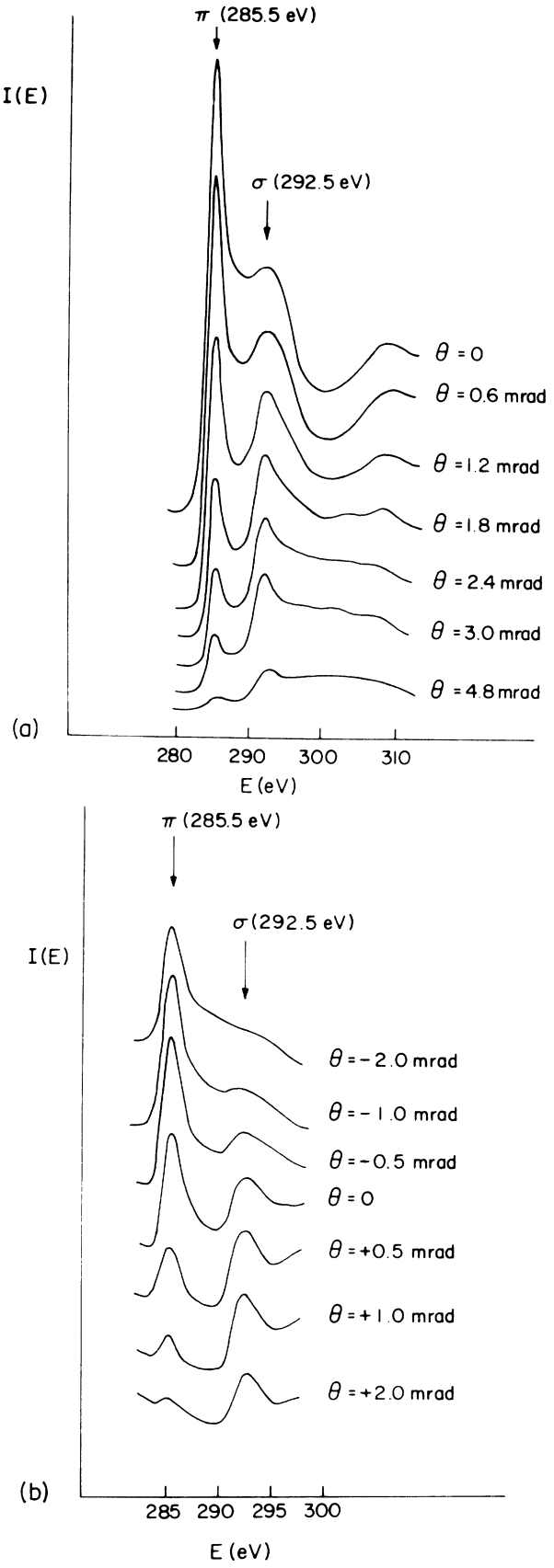

FIG. 7. (a) Microdensitometer traces across the energy axis of the spectrograph from graphite oriented at $\gamma=0$ for different values of θ. (b) Traces in energy across the spectrograph from graphite with $\gamma=-45°$ for different values of θ.

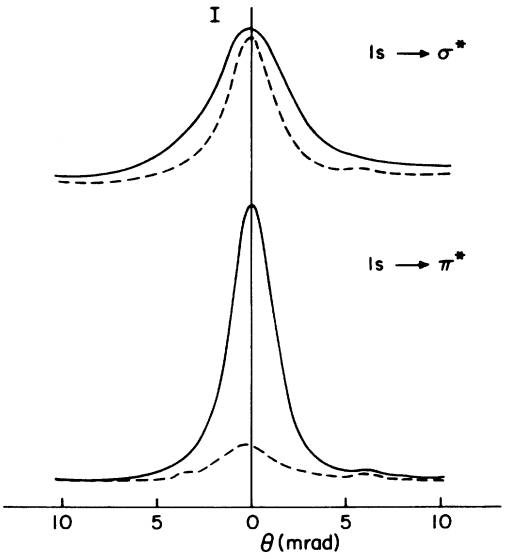

FIG. 8. Microdensitometer traces in angle across the $1s \rightarrow \pi^*$ and $1s \rightarrow \sigma^*$ peaks at the carbon K edge in graphite oriented with $\gamma=0$ (solid line). The background intensity just below the peaks is also shown (dashed line).

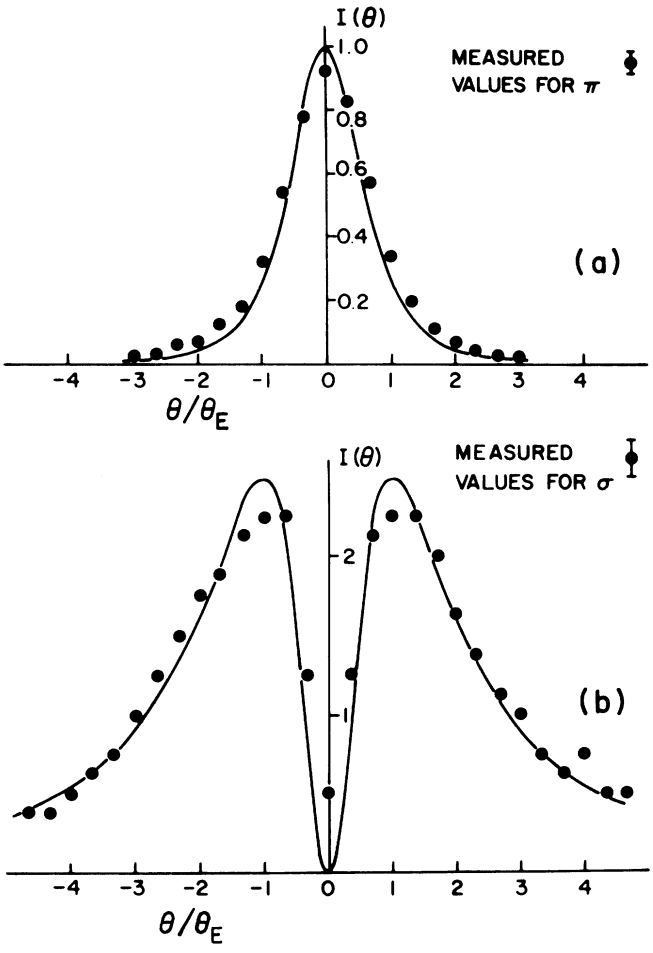

FIG. 9. (a) Measured angular distribution across the π^* in graphite with $\gamma=0$ after background subtraction (circles) and comparison with theory (solid curve). (b) Measured angular distribution across the σ^* peak in graphite ($\gamma=0$) and comparison with theory.

across the narrow entrance slit to the spectrometer. These showed up as weak vertical streaks on the spectrographs but their effect on the angular distribution was small since the background was subtracted. Figures 9(a) and 9(b) show the angular distributions across the π^* and σ^* peaks after this background subtraction for the spectrograph recorded at normal incidence. The π^* peak has a half-width less than θ_E ($=1.9$ mrad) while the σ^* has a small intensity at $\theta=0$ and reaches a maximum at about $\pm\theta_E$. Plotted on the same graphs are the theoretical angular distributions as calculated in Sec. III and scaled to facilitate comparison with the experimental data. Agreement is seen to be good, within experimental uncertainty. Figure 10 shows the angular distributions across the π^* and σ^* peaks for a sample tilted at 45°. The highly asymmetrical shapes of these curves again fit well with theory. For the π^* peak, the drop to zero intensity at $+\theta_E$ and the main maximum at $-0.4\theta_E$ are predicted accurately. For the σ^* peak the angular distribution is reflected about $\theta=0$ relative to the π^* peak so that the intensity drops to zero at $-\theta_E$. In the case of the π^* peak even the weak secondary maximum at about $+2.4\theta_E$ is observed. The absence of this secondary maximum at $-2.4\theta_E$ in the measured angular distribution for the σ^* peak can be accounted for by the poorer statistics and some multiple scattering. It is noted that the specimen thickness (~ 200 Å) as estimated from the low-loss spectrum[31] is not great enough to produce appreciable multiple scattering in the region of the carbon K edge. A small mixture of $1s \rightarrow \pi^*$ and π plasmon excitation might give some intensity at the $1s \rightarrow \sigma^*$ energy; however, this contribution is estimated as less than 10%.

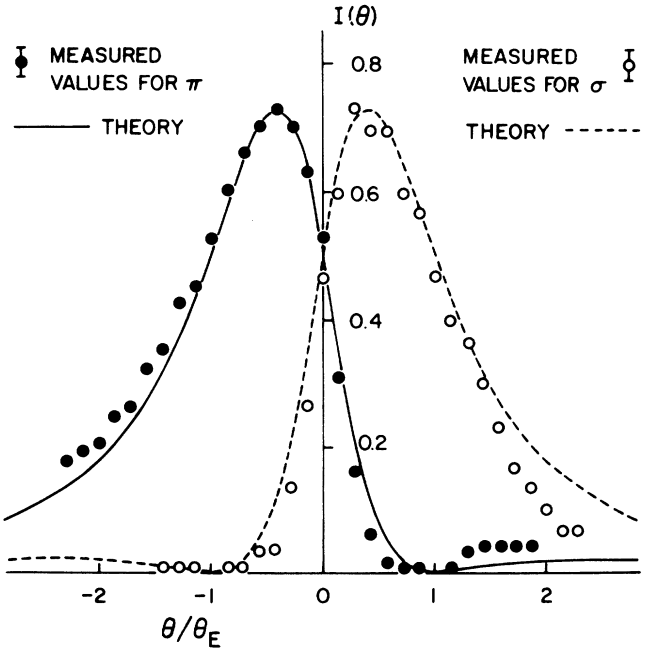

FIG. 10. Measured angular distributions across the π^* peak (solid circles) and σ^* peak (open circles) for graphite oriented at $\gamma=-45°$. Comparison with theory for the π^* peak (solid curve) and the σ^* peak (dashed curve) is also indicated.

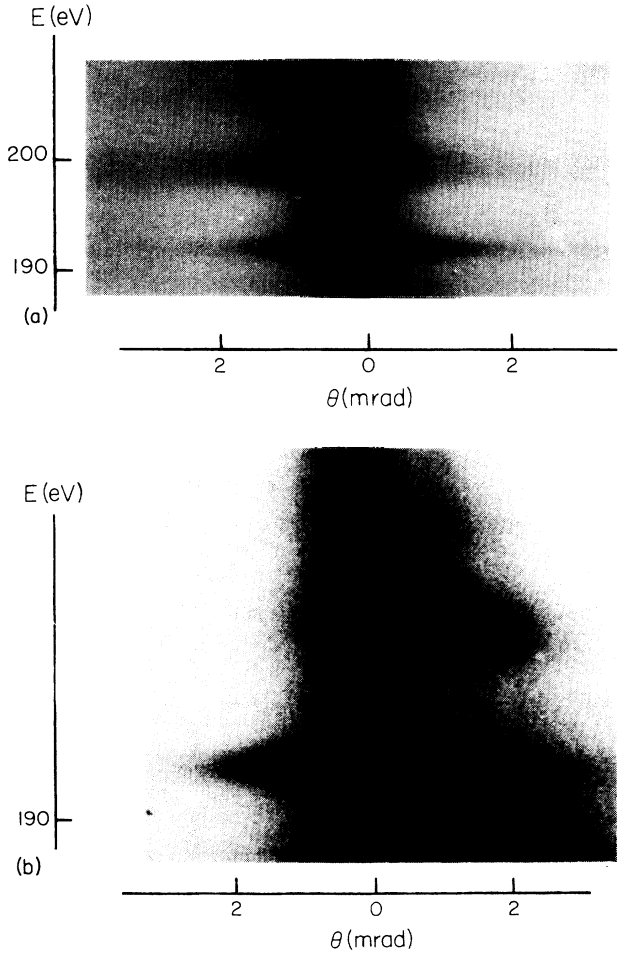

FIG. 11. (a) Spectrograph recorded on photographic plate at the boron K edge in hexagonal boron nitride at $\gamma=0$. The angular and energy scales are indicated. (b) Spectrograph at the boron K edge in BN oriented with c axis at 45° to the incident beam ($\gamma=-45°$).

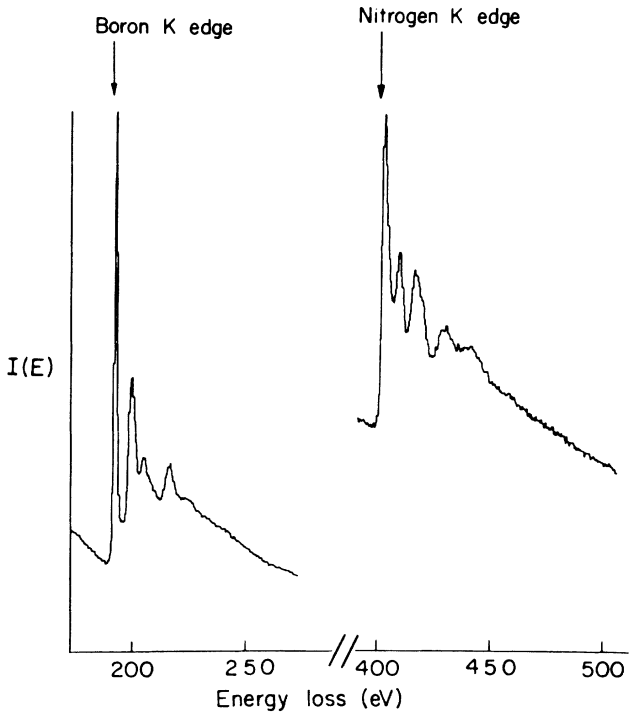

FIG. 12. Energy-loss spectrum recorded digitally at the boron K edge in BN oriented at the normal incidence.

B. Boron nitride

We now present results for boron nitride and demonstrate the close relation between these data and those for graphite. We also point out features in the core-edge spectra that are different in the two materials. We shall concentrate mainly on the boron K edge (192 eV) rather than the nitrogen K edge (402 eV) whose signal is appreciably weaker. Figures 11(a) and 11(b) show spectrographs at $\gamma=0°$ and 45°, respectively, near the boron K edge recorded from a single flake of BN about 3 μm across supported on a 100-Å amorphous carbon film. The total specimen thickness as estimated from the low-loss spectrum was around 300 Å. For normal incidence Fig. 11(a) reveals that the peak at 192 eV is concentrated at small θ compared with the 199-eV peak as in the case of the carbon K edge peak at 285.5 eV in graphite. Similarly for the sample tilted at $\gamma=45°$ in Fig. 11(b), the two peaks at 192 and 199 eV are asymmetrical about $\theta=0$. Both orientations show a weaker additional peak at 204.5 eV, which follows the angular dependence of the 199-eV peak.

Figure 12 shows the boron K edge recorded by digital scanning from a sample oriented with the c axis parallel to the incident beam. As for graphite, the size of the detector aperture effectively averages the signal over different scattering angles centered around $\theta=0$. The spectrum was used to check the linearity of the photographic plates and for calibration of the energy losses.

Figures 13(a) and 13(b) are traces along the energy-loss axis from these spectrographs for $\gamma=0°$ and 45°, respectively. The normal-incidence data [Fig. 13(a)] show the changes in amplitude of the peaks and also reveal a very weak extra peak at about 195 eV which follows the angular dependence of the 192-eV peak. For $\gamma=45°$ [Fig. 13(b)] the energy-loss spectra are seen to change completely depending on the sign of θ, as in graphite. These data for boron nitride oriented with the c axis at 45° to the beam have been reported earlier[32] but for completeness we include the results here. The weak peak at 195 eV is not seen in these data presumably because the statistics and energy resolution are just insufficient to resolve it.

The measured angular distribution at normal incidence in Fig. 14(a) for the 192-eV peak agrees well with the theoretical curve for a $1s\rightarrow\pi^*$ transition. Similarly for the 199-eV peak the angular distribution in Fig. 14(b) shows a pronounced dip at $\theta=0$ and maximum at about $\pm\theta_E$ ($=1.3$ mrad). It is noted that the experimental value does not fall to zero at $\theta=0$ as predicted by theory for a $1s\rightarrow\sigma^*$ transition and some discrepancy also occurs at higher scattering angles ($\sim 4\theta_E$). These differences can probably be accounted for by some multiple scattering and error in background subtraction although the possibility that this peak contains some π^* character should not be discounted. The general shape of the angular distribution for the 199-eV peak is consistent with σ^* symmetry.

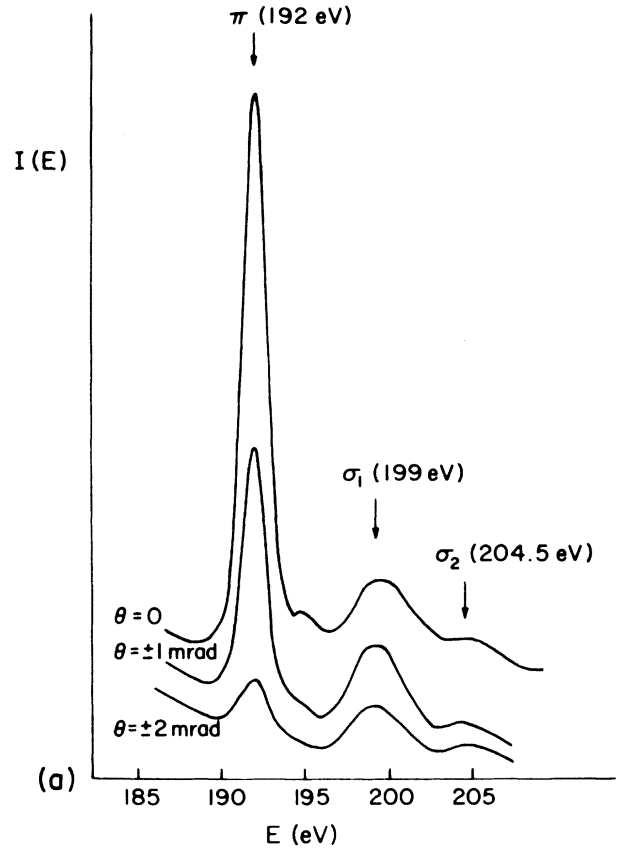

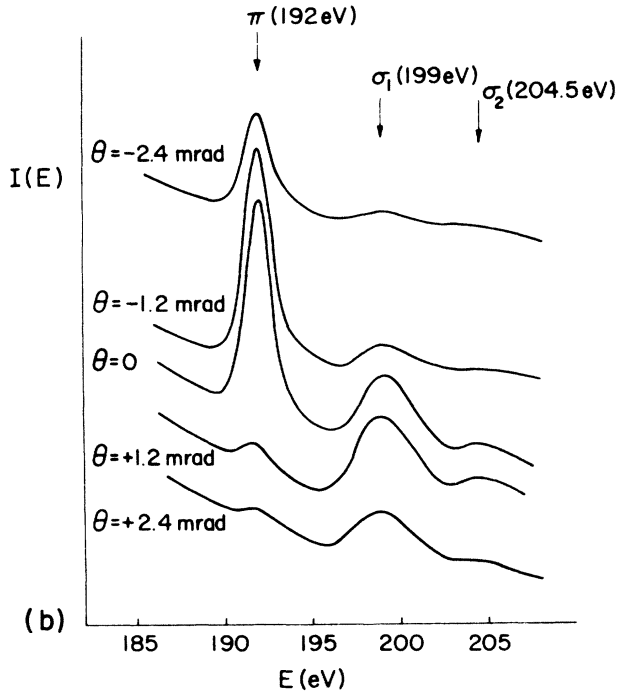

FIG. 13. (a) Traces in energy across the spectrograph from BN oriented at $\gamma=0$ for different values of θ. (b) Spectra recorded for sample oriented at $\gamma=-45°$ near the boron K edge for different values of θ.

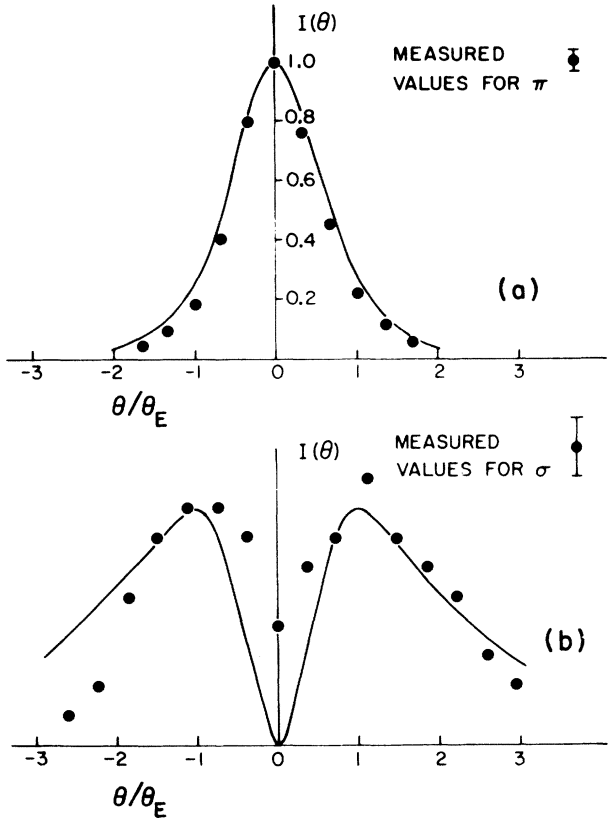

FIG. 14. (a) Measured angular distribution across the π^* peak in boron nitride with $\gamma=0$ after background subtraction (circles) and comparison with theory (solid line). (b) Measured angular distribution across the σ^* peak in BN with $\gamma=0$ and comparison with theory.

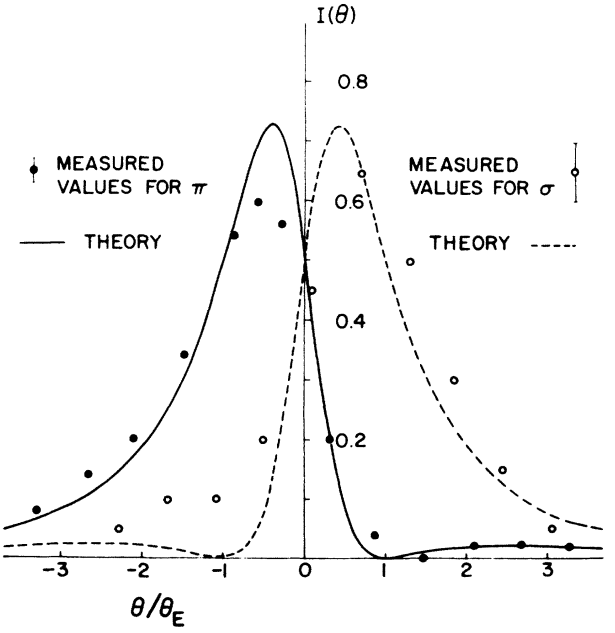

FIG. 15. Measured angular distributions across the π^* peak (solid circles) and the σ^* peak (open circles) for BN oriented at $\gamma=-45°$. Comparison with theory for the π^* peak (solid line) and the σ^* peak (dashed line) is also indicated.

Figure 15 shows traces in scattering angle across the 192- and 199-eV peaks for a sample tilted at $\gamma=45°$. As for graphite, the measured asymmetry in the peak shapes agrees with the theory for $1s\rightarrow\pi^*$ and $1s\rightarrow\sigma^*$ transitions. For the π^* peak even the weak secondary maximum at $\theta=2.4$ mrad is observed. This is not evident in the case of the σ^* peak which can again be attributed to the poorer statistics and some multiple scattering. On the basis of these results the 192-eV peak can be assigned unambiguously to a $1s\rightarrow\pi^*$ transition while the peaks at 199 and 204.5 eV can be assigned with a similar degree of confidence to $1s\rightarrow\sigma^*$ transitions. The weak peak at ~ 195 eV can be attributed to another $1s\rightarrow\pi^*$ transition though it is only visible in the normal-incidence data.

We have also obtained some data near the nitrogen K edge (402 eV) though the signal-to-noise was not as high as for the boron K edge. A spectrograph recorded on a photographic plate was taken from a sample oriented with the c axis parallel to the incident beam. Microdensitometer traces across the energy axis in Fig. 16 show similarities to the boron K edge data, though the peak at the onset of the edge is less sharp. This peak at 402 eV is concentrated at smaller scattering angles than a second and third peak at 409 and 415 eV. These results are consistent with a $1s\rightarrow\pi^*$ transition at 402 eV and $1s\rightarrow\sigma^*$ transitions at 409 and 415 eV. Such an assignment for the nitrogen K edge fits with the boron K edge data.

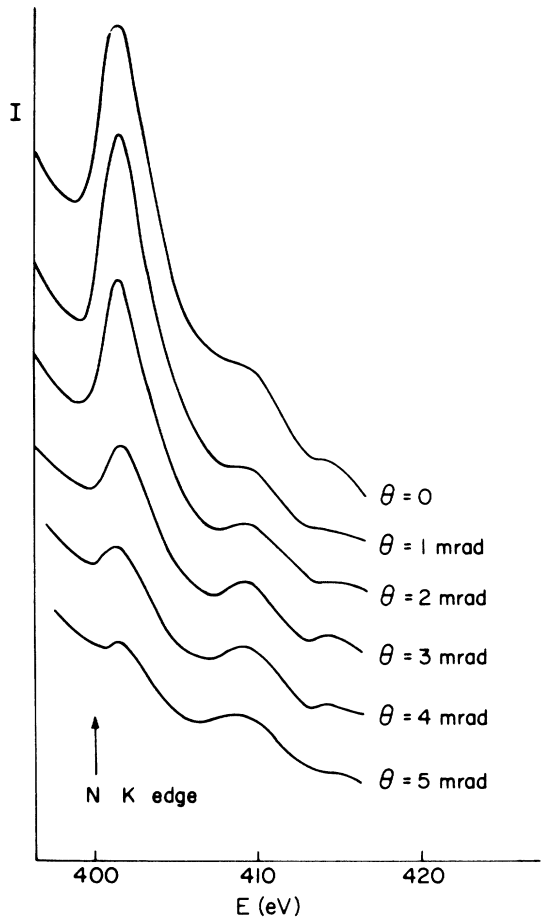

FIG. 16. Densitometer traces across the nitrogen K edge in a sample of BN oriented at normal incidence ($\gamma=0$). Spectra were obtained at different scattering angles θ.

Our data near the boron K edge may be compared with previous energy-loss measurements by Colliex *et al.*[17] and Rossouw *et al.*[16] These results, though averaged over different orientations and scattering angles, are in agreement with the present work. Colliex *et al.*[17] demonstrated that the peaks in the fine structure correspond to maxima in the density of states as calculated by Nakhmanson and Smirnov.[33] Our measurements are also in agreement with previous x-ray-absorption (quantum yield) spectra from hexagonal boron nitride by Fomichev *et al.*,[34,35] again for unoriented samples. As mentioned earlier, absorption spectra have also been obtained by Brown *et al.*[13] with polarized synchrotron radiation. Similar peaks were observed as in the present work at 192 and 195 eV but we do not agree with these authors' interpretation and this will be discussed later.

VI. DISCUSSION

A. Relation of core-edge fine structure to density of states

In the preceding sections we have described how the π^* and σ^* character of the final state can be derived from the orientation and scattering-angle dependence of the core edges. We now consider the relation between the energy-loss spectrum and the electronic structure of the materials investigated. We might expect a resemblance between peaks in the energy-loss spectrum and the density of unoccupied conduction states in the solid. However, a one-to-one correspondence of this type does not hold and the following factors should be considered. Firstly, as we have remarked earlier, our experiment probes only the state with angular momentum differing from the initial state by ± 1. For $1s$ electron excitation, only transitions to states of p symmetry are involved, so no information can be obtained about the s bands and d bands. Secondly, we may only expect structure at the core edges to reflect the density of states if the matrix element term in the cross section is energy independent. In general this is not the case and certain portions of the bands may be weighted in the spectra. The third factor to be considered when comparing core edges with density of states is the core exciton. This occurs because of the core hole which remains behind in the excitation process. Relaxation of the electron states near the core hole must be therefore taken into account. The final-state excited electron sees a potential which is nonperiodic since the excited atom has a charge increased by one. Calculations of the exciton problem with the use of localized orbitals have been carried out by Mele and Ritsko.[36] These authors show that in the case of graphite the π^* peak at the carbon K edge is shifted down by 2 or 3 eV and modified in shape. The density of states as measured by the fine structure at the core edges is therefore the local density of states and not that of the ground state of the solid. Taking these factors into account, we may compare the peaks in the spectra with peaks in the density of states derived from band-structure calculations. Differences may be attributed to excitonic effects or to inadequacies in the band-structure determinations. For ex-

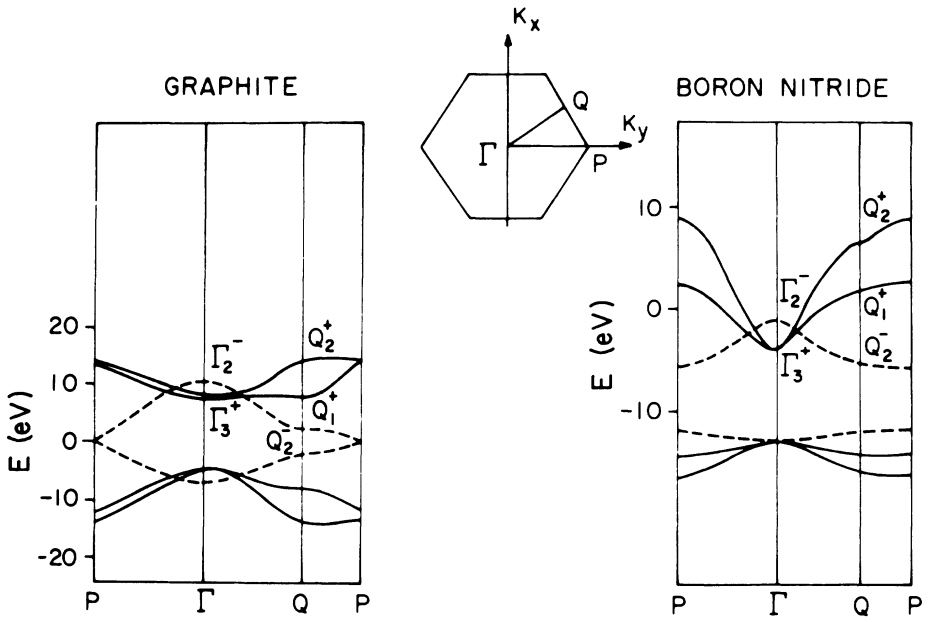

FIG. 17. Two-dimensional energy bands for the lowest unoccupied π and σ states in graphite and hexagonal boron nitride as given by Willis *et al.* (Ref. 24) and Doni *et al.* (Ref. 40), respectively. The π bands are indicated by a dashed curve and the σ bands by a solid curve. Symmetry points Γ, Q, P in the Brillouin zone are shown.

ample, at higher energies above the Fermi level ($\gtrsim 20$ eV) the conduction electrons are strongly scattered inelastically (incoherently) and have a short attenuation length. Band calculations which assume an infinite lattice may not then be valid. At these higher energies the structure in the spectrum may be best described in terms of EXAFS, i.e., backscattering of ejected electrons by nearest-neighbor atoms.

In order to estimate the energy of the unoccupied final state above that of the initial 1*s* core state we may use x-ray photoemission spectroscopy (XPS) or ultraviolet photoemission spectroscopy (UPS) data (see, for example, Brown *et al.*[13]). For graphite the data of Beyreuther *et al.*[37] give a value of 284.5 eV from the carbon *K* shell to the top of the π valence band. For boron nitride the data of Hamrin *et al.*[38] give a value of 188.6 eV from the boron *K* shell to the top of the π valence band. We also require the direct band gap between the top of the valence band and the bottom of the conduction band (~ 5.7 eV) in boron nitride.[39] It is therefore now possible to compare the peak positions in the energy-loss spectra with the energies of the maxima in the densities of states as derived from band calculations. Figure 17 shows the two-dimensional band-structure calculation of Willis *et al.*[24] and Doni *et al.*[40] for graphite and boron nitride, respectively. Strong peaks in the density of states occur at the points *Q* in the Brillouin zone where the bands are flattest. The point Γ at the center of the Brillouin zone only produces a step in the density of states because of the small volume of phase space surrounding it. The degeneracy of the occupied and unoccupied bands at the point *P* for graphite (a conductor with no band gap) is removed in the case of boron nitride which is a good insulator with a direct band gap of 5.7 eV.[39]

Tables I and II show the degree of correspondence between peaks in the energy-loss spectrum and the maxima in the calculated densities of states for graphite and boron nitride. For both materials the observed sequence of main peaks is in agreement with the sequence obtained from the band structure. In graphite a high π^* density of states near the point Q_2^- in the Brillouin zone with energy about 287.5 eV above the 1*s* level may be compared with the 285.5-eV π^* peak in the energy-loss spectrum. The σ^* bands with maxima in the density of states at Q_1^+ and Q_2^+ may be compared with peaks in the spectrum at 292.5 and 302.5 eV. The energy of the π^* peak at 285.5 eV in the spectrum is seen to lie about 2 or 3 eV lower than the value expected from the band calculations and thus is like-

TABLE I. Comparison of fine structure above *K* edge in graphite with band structure.

Maximum in density of states	Band character	Energy above carbon 1*s* level (eV) Willis *et al.*	Doni *et al.*	Energy-loss experiment
Q_2^-	π^*	287.5	287	π^* 285.5
Q_1^+	σ^*	292.5	293	σ^* 292.5
Q_2^+	σ^*	299.5	295	σ^* 302.5
				π^* 308.5

TABLE II. Comparison of fine structure above K edge in boron nitride with band structure.

Maximum in density of states	Band character	Energy above boron 1s level (eV) Doni *et al.*	Zunger *et al.*	Nakhmanson *et al.*	Energy-loss experiment
Q_2^-	π^*	195	194.5	195	π^* 192.0
					π^* 195.0
Q_1^+	σ^*	203	199.5	206	σ^* 199.0
Q_2^+	σ^*	207	203	207	σ^* 204.5

ly to be a core exciton as in graphite as discussed by Mele and Ritsko.[36] The σ^* peak at 292.5 eV in the spectrum agrees quite well with the σ^* peaks in the densities of states at about 293 and 295 eV of Doni *et al.*[39] It is possible that these peaks at Q_1^+ and Q_2^+ are not properly resolved in the present work. As remarked earlier the spectrograph of normally oriented graphite [Fig. 5(a)] shows a weak tail from the π^* peak at 285.5 eV overlapping with the σ^* peak at 292.5 eV. It is interesting to note that the band calculations also show such an overlap of π^* and σ^* bands (Fig. 17). The observed peaks in the spectrum at 302.5 eV (σ^*) and 308.5 (π^*) can probably be attributed to higher-energy bands in the calculations of Willis *et al.*[24]

In boron nitride the π^* peak at threshold in the energy-loss spectrum is about 2 or 3 eV lower than the values expected from the band-structure maximum at Q_2^- in the Brillouin zone. This difference can again be attributed to a core exciton. Table II contains the energies of the band maxima derived from the computations of Zunger *et al.*,[39] Doni *et al.*,[40] and Nakhmanson *et al.*[33] The energies above the boron 1s level were determined from the photoemission data of Hamrin[38] as described above. The weak π^* peak at about 195 eV in the energy-loss spectrum which is close to the one at 194.5 eV observed by Brown *et al.*[13] does not seem to correspond to a maximum in the density of states and could perhaps be a second core exciton (suggested to us by F. C. Brown). If this is the case the difference in energy between the first and second exciton could give the exciton binding energy. Evidence for the existence of a core exciton is also present in the data of Fomichev *et al.*[35,36] These authors find a sharp peak at almost the same energy in the x-ray emission (191.3 eV) and absorption spectra (191.8 eV) from boron nitride. They therefore deduce that the emission peak arises from the downward transition of electrons from the first excited 2p level of the boron atom.

The σ^* peak at 199 eV in the energy-loss spectrum seems to correspond to the maximum at Q_1^+ in the band calculations. Similarly the 204.5-eV σ^* peak in the spectrum can be assigned to the maximum at Q_2^+. There is again evidence that the energies of the σ^* peaks are higher in the band calculations by 2 or 3 eV. The results indicate that peaks in the energy-loss spectrum of graphite and boron nitride can be matched semiquantitatively with peaks in the calculated densities of states. In fact there is some evidence that all the peaks are shifted down in energy by approximately the same amount by the core exciton or local density-of-states effects. Discrepancies between various band calculations make an exact comparison difficult. However, it seems clear that the shapes of peaks are modified substantially by excitonic effects.[36] The peak at threshold is found to be greatly enhanced and narrowed. On the other hand, the results demonstrate that certain features of the band structure are preserved in the core-edge spectrum.

B. Comparison with synchrotron studies

As mentioned in Sec. II we expect our experiments to be similar to studies with polarized synchrotron radiation. It is interesting that our observations differ from those of Brown *et al.*[13] for boron nitride. These authors report a peak at the boron K edge (192 eV), which does not change appreciably for the two crystal orientations investigated (the electric field vector in the layer plane and inclined at 23° to the layer plane). They attribute this peak to a $1s \rightarrow \sigma^*$ transition. A peak at 194.5 eV in their data was found to increase in the 23° orientation and is attributed to a $1s \rightarrow \pi^*$ transition. Our observations, discussed above, show that both the 192- and 195-eV peaks are polarized along the c axis (π^*). We have considered that the energy-loss technique could give rise to different excitation modes that for the synchrotron studies. Specifically, fast electrons develop a transverse electric field component as well as a longitudinal component as the speed becomes relativistic. Eventually losses due to the excitation of Čerenkov radiation will arise. If the losses reported here were due primarily to this mechanism, then the polarization would reflect asymmetry at 90° to the interpretation given above. The condition that Čerenkov enhancement be significant is $\epsilon(\omega)\beta^2 \geq 1$, where $\beta = v/c$, which for 75-keV electrons implies $\epsilon(\omega) \geq 4$. We have modeled the dielectric constant[41,42] for the fine structure with reasonable values for the oscillator strength,[43] damping,[34] and resonance frequency. The result is sufficiently far from the Čerenkov enhancement condition that our data cannot be explained in this way. Similarly, surface excitations which also contain transverse components are excluded for the same reason. Details of this evaluation are given in the Appendix.

Although the reasons for the discrepancies between the synchrotron data and ours are not clear, we note that some difficulties have previously been encountered with x-ray polarization measurements. Results of an experiment on the Se L edge originally attributed to our orientation dependence[14] were later shown to arise from holes in the sample.[15] Problems are also likely to occur if the sample

is too thick and uncertainties may exist in determining the degree of polarization of the synchrotron beam. We also note that in our energy-loss studies it was possible to view the regions of the sample under investigation at high magnification in the electron microscopic and to characterize them accurately using diffraction patterns. We can verify that the samples were single crystal in the required orientation.

VII. CONCLUSIONS

We have demonstrated that inelastic scattering of fast electrons can be used to deduce the polarization of unoccupied states in anisotropic crystals. Fine structure in the region of the core edges has been shown to vary with crystal orientation and momentum transfer in the expected way for graphite and boron nitride. In many ways the technique complements x-ray spectroscopy in that it is possible to carry out these studies on small well-characterized samples rather than bulk materials. Also low-loss studies may be carried out at the same time with the energy-loss spectroscopy, and this can provide useful additional information. The direction of the momentum transfer with respect to the unoccupied valence states not only depends on the crystal orientation, as for the synchrotron studies, but also on the scattering angle. So, for a given crystal orientation there is enough information to identify the character of the final state if the scattered electron intensity is measured as a function of both energy-loss and scattering angle. Such data can be recorded in parallel using for example a photographic plate. This offers great sensitivity and any asymmetries in the angular distribution of the core excitations for a tilted sample at once indicate anisotropy. With more than one crystal orientation, conclusions about the symmetry of the final states can be reached even more readily. Comparison of the core edges with band calculations for graphite and boron nitride show the degree of similarity between the ground-state density of states and the density of states in the presence of the core hole. Although differences occur in the peak shapes and positions, general correspondence is found between the sequence of the π^* and σ^* maxima. There is evidence that the core exciton effects shift different peaks in the density of states by about the same amount towards lower energies. It would be interesting to see if this is the case for other materials.

ACKNOWLEDGMENTS

We are grateful to Professor F. C. Brown for helpful discussions. Financial support from the National Science Foundation through the Cornell University Materials Science Center is gratefully acknowledged (R.D.L. and J.S.). Enhancement of the experimental capability (P.L.F.) was supported by the National Science Foundation through Grant No. DMR-78-09204.

APPENDIX: POSSIBLE ČERENKOV ENHANCEMENT AT THE CORE EDGE IN BORON NITRIDE

When the real part of the dielectric constant ϵ_1 exceeds β^{-2}, Čerenkov enhancement can occur. Here β is the ratio of the electron velocity to that of light, so for 75-keV electrons $\beta \sim 0.5$ and $\epsilon_1 \gtrsim 4$.

The complex dielectric constant can be written in terms of the oscillator strength f_T assuming there is no significant momentum-transfer dependence. We have

$$\epsilon(\omega)=\epsilon_1(\omega)+i\epsilon_2(\omega)=1-\frac{\omega_p^2 f_T(\omega)}{\omega^2-\omega_T^2+i\omega/\tau} . \quad \text{(A1)}$$

Here ω is the frequency (or energy loss), and f_T is the oscillator strength for the transition from the $1s$ subshell to the π^* antibonding state and the corresponding transition energy, $\omega_T = 192$ eV. ω_p is the plasma energy for N atoms per unit volume

$$\omega_p=\left[\frac{4\pi Ne^2}{n}\right]^{1/2} \simeq 15$$

(in units of eV), τ is the relaxation time for the scattering process, and τ^{-1} corresponds to the width of the resonance in the energy-loss spectrum. Experimentally this is 0.6 eV for the $1s \rightarrow \pi^*$ in boron nitride. The oscillator strength in the 192-eV peak may be estimated from the theoretical differential oscillator strength[43] together with the measured spectrum. We estimate f_T as about 0.05.

The maximum value of ϵ_1 is obtained from Eq. (A1):

$$\epsilon_1^{\max}=1+\frac{\omega_p^2 f_T}{2\omega_T\tau^{-1}} .$$

This gives $\epsilon_1^{\max} \simeq 1.05$ which is far from the Čerenkov condition.

*Present address: Division of Biomedical Engineering, National Institutes of Health, Bethesda, MD 20205.

†Present address: Motorola, Inc., 5005 E. McDowell Rd., Phoenix, AZ 85008.

[1]M. S. Isaacson, J. Chem. Phys. 56, 1813 (1972).

[2]D. Johnson, Rad. Res. 49, 63 (1972).

[3]C. Colliex and B. Jouffrey, Philos. Mag. 25, 491 (1972).

[4]R. F. Egerton and M. J. Whelan, J. Electron Spectrosc. Relat. Phenom. 3, 232 (1974).

[5]R. F. Egerton and M. J. Whelan, Philos. Mag. 30, 739 (1974).

[6]J. J. Ritsko, N. O. Lipari, P. C. Gibbons, and S. E. Schnatterly, Phys. Rev. Lett. 37, 1068 (1976).

[7]H. Raether, in *Solid State Excitations by Electrons*, Vol. 38 of *Springer Tracts in Modern Physics*, edited by G. Höhler (Springer, Berlin, 1965), p. 84.

[8]J. Daniels, C. V. Festenberg, H. Raether, and K. Zeppenfeld, in *Optical Constants of Solids by Electron Spectroscopy*, Vol. 54 of *Springer Tracts in Modern Physics*, edited by G. Höhler (Springer, Berlin, 1970), p. 77.

[9]C. H. Chen and J. Silcox, Phys. Rev. B 16, 4246 (1977).

[10]C. H. Chen, Phys. Status Solidi B 83, 347 (1977).

[11]M. G. Bell and W. Y. Liang, Adv. Phys. 25, 53 (1976).

[12]W. Y. Liang and S. L. Cundy, Philos. Mag. 19, 1031 (1969).
[13]F. C. Brown, R. F. Bachrach, and M. Skibowski, Phys. Rev. B 13, 2633 (1976).
[14]E. A. Stern, D. E. Sayers, and F. W. Lytle, Phys. Rev. Lett. 37, 298 (1976).
[15]S. M. Heald and E. A. Stern, Phys. Rev. B 16, 5549 (1977).
[16]C. J. Rossouw, R. F. Egerton, and M. J. Whelan, Vacuum 26, 427 (1977).
[17]C. Colliex, *Analytische Elektronenmikroskopie* (Kontron, Munich, 1976), p. 204.
[18]B. M. Kincaid, A. E. Meixner, and P. M. Platzman, Phys. Rev. Lett. 40, 1296 (1978).
[19]H. A. Bethe, Ann. Phys. 5, 325 (1930).
[20]M. Inokuti, Rev. Mod. Phys. 43, 297 (1971).
[21]U. Fano and J. W. Cooper, Rev. Mod. Phys. 40, 441 (1968).
[22]J. M. Ziman, *Principles of the Theory of Solids* (Cambridge University Press, Cambridge 1972).
[23]G. H. Curtis and J. Silcox, Rev. Sci. Instrum. 42, 630 (1971).
[24]R. F. Willis, B. Fitton, and G. S. Painter, Phys. Rev. B 9, 1926 (1974).
[25]R. D. Leapman and V. E. Cosslett, J. Phys. D 9, L29 (1976).
[26]J. J. Ritsko, S. E. Schnatterly, and P. C. Gibbons, Phys. Rev. Lett. 32, 671 (1974).
[27]C. J. Rossouw, Ph.D. thesis, University of Oxford, 1977 (unpublished).
[28]P. E. Batson and A. J. Craven, Phys. Rev. Lett. 42, 893 (1979).
[29]R. F. Egerton, Philos. Mag. 30, 739 (1974).
[30]A. B. Ray, in *Proceedings of the 37th Annual Meeting of the Electron Microscopy Society of America,* edited by G. W. Bailey (Claitor's Publishing Division, Baton Rouge, 1979), p. 522.
[31]R. D. Leapman and V. E. Cosslett, Philos. Mag. 33, 1 (1976).
[32]R. D. Leapman and J. Silcox, Phys. Rev. Lett. 42, 1361 (1979).
[33]N. S. Nakhmanson and V. P. Smirnov, Fiz. Tverd. Tela (Leningrad) 13, 2388 (1971) [Sov. Phys.—Solid State 13, 2763 (1972)].
[34]V. A. Fomichev, Fiz. Tverd. Tela (Leningrad) 9, 3167 (1967) [Sov. Phys.—Solid State 9, 2496 (1968)].
[35]V. A. Fomichev and M. A. Rumsh, J. Phys. Chem. Sol. 29, 1015 (1968).
[36]E. J. Mele and J. J. Ritsko, Phys. Rev. Lett. 43, 68 (1979).
[37]C. Beyreuther and G. Wiech, in *Vacuum Ultraviolet Radiation Physics,* edited by E. E. Koch, R. Haensel, and C. Kunz (Vieweg, Braunschweig, 1974), p. 517.
[38]K. Hamrin, G. Johansson, U. Gelius, C. Nordling, and K. Siegbahn, Phys. Scr. 1, 277 (1970).
[39]A. Zunger, A. Katzir, and A. Halperin, Phys. Rev. B 13, 5560 (1976).
[40]E. Doni and G. Pastori Parravicini, Nuovo Cimento B 63, 117 (1969).
[41]J. Jelly, *Čerenkov Radiation and its Applications* (Pergamon, New York, 1958).
[42]C. H. Chen, Ph.D. thesis, Cornell University, 1974 (unpublished).
[43]R. D. Leapman, Ultramicroscopy 3, 413 (1979).

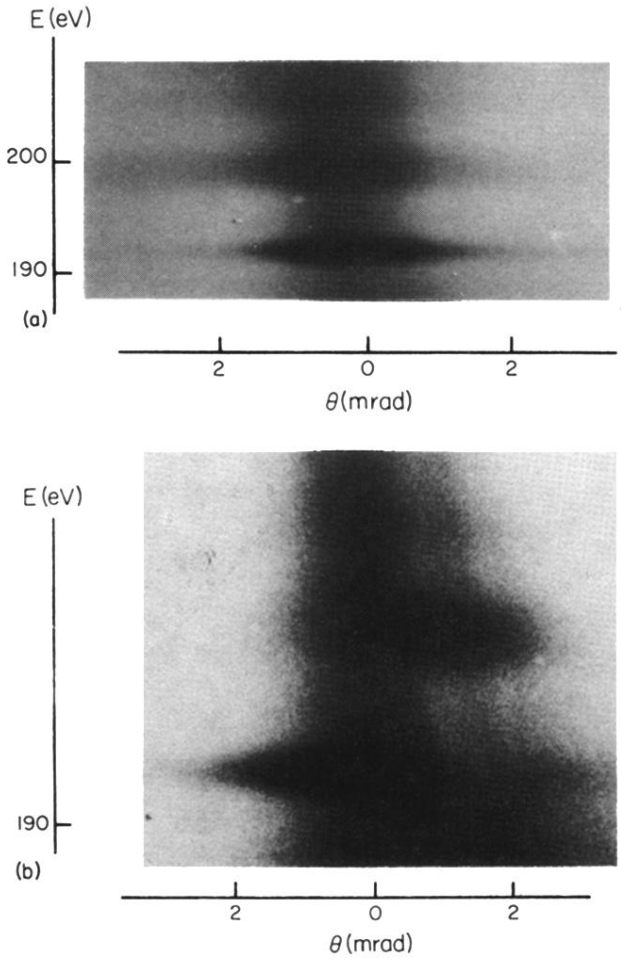

FIG. 11. (a) Spectrograph recorded on photographic plate at the boron K edge in hexagonal boron nitride at $\gamma=0$. The angular and energy scales are indicated. (b) Spectrograph at the boron K edge in BN oriented with c axis at 45° to the incident beam ($\gamma=-45°$).

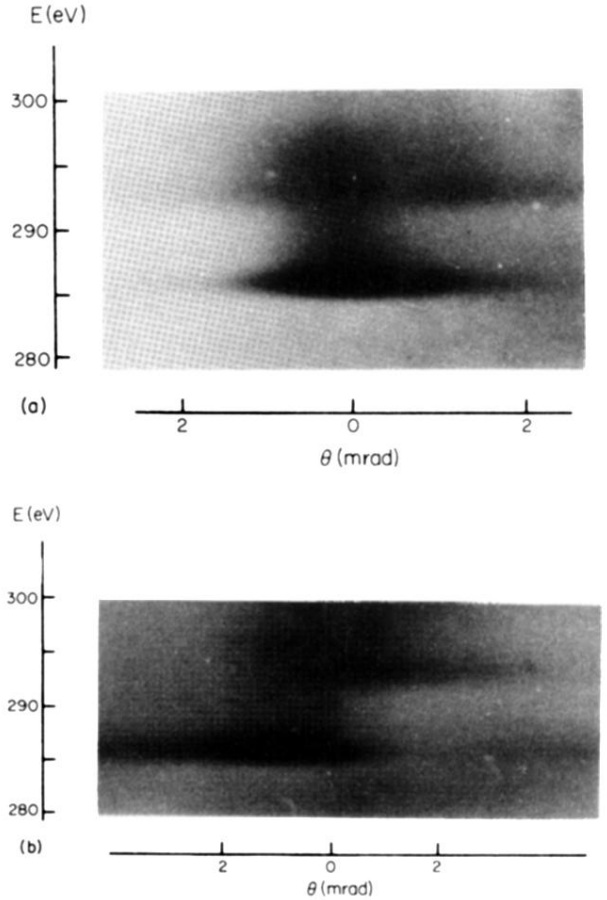

FIG. 5. (a) Spectrograph recorded on photographic plate at the carbon K edge in graphite oriented at normal incidence ($\gamma=0$). The angular and energy scales are indicated. (b) Spectrograph at the carbon K edge in graphite oriented with c axis at 45° to the incident beam direction ($\gamma=45°$).